

1 **Development and validation of the Terrain Stability model for assessing landslide instability**
2 **during heavy rain infiltration.**

3 1. Alfonso Gutiérrez-Martín^[1] Miguel Ángel Herrada^[2], José Ignacio Yenes Gallego^[3],
4 Ricardo Castedo Ruiz^[4]

5 ^[1] Dr. Arquitecto, Escuela Superior de Arquitectura; Universidad de Málaga, España. E-mail:
6 alfgutmar@uma.es

7 ^[2] Catedrático de Universidad, Escuela Superior de Ingenieros de la Universidad de Sevilla.
8 España. E-mail: herrada@us.es

9 ^[3] Dr. Ingeniero José Ignacio Yenes Gallego, Jefe de Unidad, Dirección General de
10 Infraestructuras, MINISDEF, Madrid, España. E-mail: jyengal@et.mde.es

11 ^[4] Dr. Ingeniero Ricardo Castedo Ruiz, Departamento de Ingeniería Geológica y Minera,
12 Universidad Politécnica de Madrid, España. E-mail: ricardo.castedo@upm.es

13 **Abstract**

14 Slope stability is a key topic, not only for engineers but also for politicians, due to the
15 considerable monetary and human losses that landslides can cause every year. In fact, it is
16 estimated that landslides have caused thousands of deaths and economic losses amounting to
17 tens of billions of euros per year around the world (Guha-Sapir et al., 2004; Kahn, 2005; Toya
18 and Skidmore, 2007; Raghuvanshi et al., 2014; Girma et al., 2015). The geological stability of
19 slopes is affected by several factors, such as climate, earthquakes, lithology and rock
20 structures, among others. Climate is one of the main factors, especially when large amounts of
21 rainwater are absorbed in short periods of time. Taking into account this issue, we developed
22 an innovative analytical model using the limit equilibrium method supported by a geographic
23 information system (GIS). This model is especially useful for predicting the risk of landslides in
24 scenarios of heavy unpredictable rainfall. The model, hereafter named 'Terrain Stability' or TS
25 is a 2D model, programmed in MATLAB and includes a steady state hydrological term. Many
26 variables measured in the field – topography, precipitation, type of soil – can be added,
27 changed or updated using simple input parameters. To validate the model, we applied it to a
28 real example, that of a landslide which resulted in human and material losses (collapse of a
29 building) at Hundidero, La Viñuela (Málaga), Spain, in February 2010.

30 **Keywords:** Rainfall, Slope, Limit equilibrium model, algorithm and critical surface.

31 **1. Introduction**

32 Landslides, one of the natural disasters, have resulted into significant injury and loss to the
33 human life and damaged property and infrastructure throughout the world (Varnes, 1996;
34 Parise and Jibson, 2000; Dai et al., 2002; Crozier and Glade, 2005). Normally, heavy rainfall,
35 high relative relief and complex fragile geology with increased manmade activities, have
36 resulted in increased landslide (Gutiérrez-Martín, 2015). It is essential to identify, evaluate
37 and delineate landslide hazard prone areas for proper strategic planning and mitigation
38 (Bisson et al., 2014). Therefore, to delineate landslide susceptible slopes over large areas,
39 landslide hazard zonation (LHZ) techniques can be employed (Anbalagan, 1992; Guzzetti et al.,

40 1999; Casagli et al., 2004; Fall et al., 2006). Landslides are resulted because of intrinsic and
41 external triggering factors. The intrinsic factors are mainly; geological factors, geometry of the
42 slope (Hoek and Bray, 1981; Ayalew et al., 2004; Wang and Niu, 2009).

43 The external factors which generally trigger landslides are rainfall (Anderson, 1985; Collison et
44 al., 2000; Dai and Lee, 2001). Several LHZ techniques have been developed over the past and
45 these can be broadly classified into three categories; expert evaluation, statistical methods
46 and deterministic approaches (Wu and Sidle, 1995; Leroi, 1997; Guzzetti et al., 1999; Inverson,
47 2000; Crosta and Frattini, 2003; Casagli et al., 2004; Fall et al., 2006; Lu and Godt, 2008; Rossi
48 et al., 2013; Raia et al., 2014; Canili et al., 2018; Zhang et al.; 2018). Within these models, we
49 want to highlight the empirical models that are based on rainfall thresholds (Wilson, 1997;
50 Aleotti, 2004; Gruzzetti et al., 2007; Martelloni et al., 2011). Each of these LHZ techniques has
51 its own advantage and disadvantage owing to certain uncertainties on account of factors
52 considered or methods by which factor data are derived (Carrara et al., 1995). Limit
53 equilibrium types of analyses for assessing the stability of earth slopes have been in use in
54 geotechnical engineering for many decades. The idea of discretizing a potential sliding mass
55 into vertical slices was introduced in the 20th century. During the next few decades, Fellenius
56 introduced the Ordinary method of slices (Fellenius, 1936). In the mid1950s Janbu and Bishop
57 developed advances in the method (Janbu, 1954; Bishop, 1955). The advent of electronic
58 computers in the 1960's made it possible to more readily handle the iterative procedures
59 inherent in the method, which led to mathematically more rigorous formulations such as
60 those developed by Morgenstern and Price and by Spencer (Morgenstern and Price, 1965;
61 Spencer, 1967).

62 Until the 1980s, most stability analyses were performed by graphical methods or by using
63 manual calculators. Nowadays, the quickest and most detailed analyses can be performed
64 using any ordinary computer (Wilkinson et al., 2002). There are other types of software based
65 on the modeling of the probability of occurrence of shallow landslides LHZ, in more extensive
66 areas using GIS technology and MDE, as is the case of deterministic software TRIGRS ,SINMAP,
67 R-SHALSTAB, GEOTop/GEO-FS, R-Slope-stability among others (Montgomery and Dietrich,
68 1998; Pack et al., 2001; Rigon et al., 2006; Simoni et al., 2008 ; Baum et al., 2008; Mergili et
69 al., 2014a; Mergili et al., 2014b; Michel et al., 2014; Reid et al., 2015; Alvioli and Baum, 2016;
70 Tran et al., 2018). They are widely used models for calculating the time and location of the
71 occurrence of shallow landslides caused by rainfall at the territorial level; some even in three
72 dimensions, in order to obtain a probabilistic interpretation of the factor of safety. Currently
73 other approaches / theoretical studies for landslide prediction are used (for triggering and / or
74 propagation) (Martelloni and Bagnoli, 2014; Martelloni et al., 2017). The idea of discretizing
75 through this tool proposed (TS), the potential slip mass in the critical profile of the slope, once
76 we have detected through the HZD programs unstable areas, is one of the achievements of
77 this model. This calculation tool is not limited to shallow landslides and debris flows, but allows
78 analysis of deep and rotational landslides, which others do not allow. Using the infiltration
79 factor of Spencer r_u we introduce the hydrological variable by infiltration to the stability
80 calculation of the slope.

81 Limit equilibrium types of analyses for assessing the stability of earth slopes have been in use
82 in geotechnical engineering for las year. Currently, the vast majority of stability analyses using

83 **this method of equilibrium limit** are performed with commercial software like SLIDE V5,
84 SLOPE/W, Phase2, GEO-Slope, GALENA, GSTABL7, GEO5 and GeoStudio, among others
85 (Gonzalez de Vallejo et al., 2002; Acharya et al., 2016a; Acharya et al., 2016b; Johari and
86 Mousavi, 2018) Other models of slope stability based on the theory of limit equilibrium are still
87 being studied, as is the case of the SSAP model (Borselli, 2012), but in this case a general
88 equilibrium method model is applied. **Second, sometimes in this commercial software, the**
89 **introduction of the parameters to perform the calculations, are not very interactive.** For the
90 stability analysis, different approaches can be used, such as the limit equilibrium methods
91 (Cheng et al., 2007; Liu et al., 2015), the finite elements method (Griffiths et al., 2007;
92 Tschuchnigg et al., 2015; Griffiths, 2015) and the dynamic method (Jia et al., 2008), among
93 others. Limit equilibrium methods are well known, and their use is simple and quick. These
94 methods allow us to analyse almost all types of landslides, such as translational, rotational,
95 topple, creep and fall, among others (Zhou and Cheng, 2013). **For the stability analysis,**
96 **different approaches can be used, such as the limit equilibrium methods (Zhu et al., 2005;**
97 **Cheng et al., 2007; Verruijt, 2010; Liu et al., 2015), the finite elements method (Griffiths et al.,**
98 **2007; Tschuchnigg et al., 2015; Griffiths, 2015) and the dynamic method (Jia et al., 2008)**
99 **among others (SSAP 2012, Slide V5-2018).** Also, limit equilibrium methods can be combined
100 with probabilistic techniques [Stead et al., 2000] or with other models, like stability analysis of
101 coastal erosion (Castedo et al., 2012). However, they are limited in general to 2D planes and
102 easy geometries. Numerical methods – finite elements methods – give us the most detailed
103 approach to analysing the stability conditions for the majority of evaluation cases, including
104 complex geometries and 3D cases. Nevertheless, they present some problems, such as their
105 complexity, data introduction, mesh size effect and the time and resources they require
106 (Ramos Vásquez, 2017).

107 **Software such as the programmes mentioned above provides useful tools for determining the**
108 **stability through the F_s (safety of factor)** and for giving the most probable breakage (shearing)
109 surfaces. This technique is fast and allows the field or emergency engineer to make timely
110 decisions. Although this methodology is only available in some current software (Slide V 5.0,
111 STB 2010, Geo-Slope), and based on limit equilibrium methods, it is highly recommended
112 because of its reliability for representing real conditions in the field (Chugh, 1981). This rain
113 infiltration produces a substantial reduction of cohesion (a key soil parameter for stability) that
114 cannot be reproduced by actual software and then several real situations cannot be predicted.

115 Delft University has developed a well-known and free software programme to analyse
116 landslides, the STB 2010 (Verruijt, 2010). This programme is based on a limit equilibrium
117 technique, using a modified version of Bishop's method to calculate the F_s only for circular
118 failures. It is a user-friendly tool, but it does not allow the calculation of water infiltration on a
119 hillside. This is a critical point, as it is well known that rainfall infiltration is one of the main
120 causes of landslides worldwide (Michel et al., 2015). Reviewing these issues, a new solution
121 must be developed for cases where landslides are linked to heavy rainfall. In this study, we
122 developed a new model and programmed it using MATLAB. **The primary result of this model**
123 **was a stability index, namely the minimum F_s ,** based on the limit equilibrium technique, in this
124 case the Bishop's method. The model also provides a possible failure curve **and surface area,**
125 **including the infiltration effects,** which can be used to coincide with analysis of the actual

126 event as tested with field data. Topographical data can also be introduced into the model from
 127 the digital elevation model (DEM) in a GIS.

128 2. Terrain Stability model development

129 In the model we developed the Terrain Stability (TS) model, we used the limit equilibrium
 130 technique for its versatility, calculation speed and accuracy. An analysis can be done studying
 131 the whole length of the breakage (shearing) zone or just small slices. Starting with the original
 132 method of slides developed by Petterson and Fellenius (1936), some methods are more
 133 accurate and complex (Spencer 1967; Morgenstern and Price, 1965) than others (Bishop, 1955
 134 and Janbú, 1954). Using Spencer's method (Spencer, 1967; Chung, 1986) here would mean
 135 dividing our slope into small slices that must be computed together. This method is divided
 136 into two equations, one related to the balance of forces and the other to momentum.
 137 Spencer's method imposes **equilibrium** not only for the forces but also for the momentum on
 138 the surface of the rupture. If the forces for the entire soil mass are in equilibrium, the sum of
 139 the forces between each slice must be also equal to zero. Therefore, the sum of the horizontal
 140 forces between slices must be zero as well as the sum of the vertical ones (equations 1 and 2).

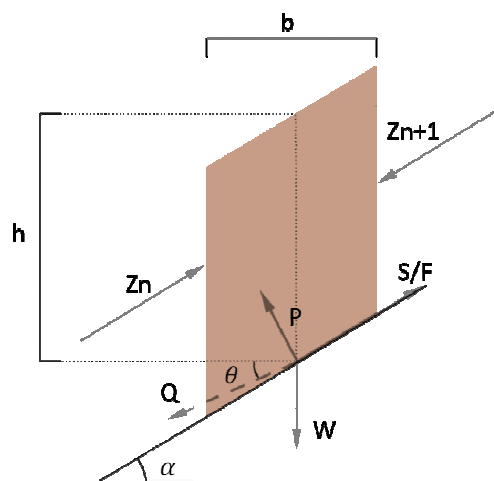
$$141 \quad \sum[Q \cos \theta] = 0 \quad (1)$$

$$142 \quad \sum[Q \sin \theta] = 0 \quad (2)$$

143 In this equation, Q is the resultant of the pair of forces between slices, and θ is the angle of the
 144 resultant (Figure 1). From this, it can be stated that the sum of the moments of the forces
 145 between slices around the critical rotation centre is zero, conformed to equation 3:

$$146 \quad \sum[QR \cos(\alpha - \theta) = 0] \quad (3)$$

147 When the R is the radius of the curvature, α is the angle of the slope referred to each slice. This
 148 takes into account that the sliding surface is considered circular, so the radius of the curvature
 149 is constant.



150

151 **Figure 1.** Representation of the forces acting on a slice, considered in Spencer's method (Spencer, 1967).

152 W is the external vertical loads; Z_n and Z_{n+1} are the forces acting on the left- and right-hand side of each

153 slice, respectively, with their horizontal and vertical components; P and S are the normal and tangential
154 forces at the base of the slice; α is the angle of the slope referred to each slice, b is the slice width and h
155 is the mean height of slice (if the height is not constant).

156 These equations must be solved to get the F_s , and tilt angles of the forces among the slices (θ).
157 To solve these equations, an iterative method is required until a limiting error is reached. Once
158 F_s and θ are calculated, the remaining forces are also obtained for each slice. Spencer's
159 method is considered very accurate and suitable for almost all kinds of slope geometries and
160 may be the most complete equilibrium procedure. It may also be the easiest method for
161 obtaining the F_s (Duncan and Wright, 2005). Depending on the type of slope analysed, this
162 model is able to establish the failure curve following the typical rotational circle, among other
163 uses (Verruijt, 2010).

164 The F_s , classically defined as a ratio of stabilizing and destabilizing forces, determines the
165 stability of a slope as follows:

$$166 \quad F_s = \frac{\Sigma(\text{Forces standing against/oppose sliding})}{\Sigma(\text{Forces that induce sliding})} \quad (4)$$

167 According to limit equilibrium methods, the two equilibrium conditions (forces and moments)
168 must be satisfied. Taking into account these elements, the F_s is then obtained from the
169 following expression (Spencer, 1967):

$$170 \quad F_s = \frac{1}{\Sigma W \sin \alpha} \Sigma [c' b \sec \alpha + \tan \phi' (W \cos \alpha - u b \sec \alpha)] \quad (5)$$

171 Where ϕ' is the friction angle at the fracture surface, u is the pore pressure at the fracture
172 zone, c' is the soil cohesion, α is the angle at the base of the slice, W is the external vertical
173 forces and b the width of the slice. According to equations (4) and (5), the slope FOS (F_s) can
174 be considered unstable if its value is lower than 1, or stable if it is equal or higher than 1. It
175 should be noted that, when applying the factor in the engineering and architecture fields, the
176 limiting value tends to be higher than 1, with common values being 1.2 or even up to 1.5
177 (Burbano et al., 2009), security coefficients that include The European technical regulations
178 and, specifically, the technical regulations of Spanish application (table 2.1, of the DB-C of the
179 CTE, or Technical Code of the Building) among others. This is just a confidence measure for
180 your calculations. The F_s can also be defined as the ratio between the shear strength (τ), based
181 on the cohesion and the angle of friction values, and the shear stress, based on the cohesion
182 and the internal friction angle required to maintain the equilibrium (τ_{mb}).

183 As mentioned, the minimum F_s to consider a slope stable is equal to 1. However, several
184 authors (Yong et al., 1977; Van Westen and Terlien, 1996) suggest that the angle of a slope
185 would have to be defined by a value of the F_s superior to the unity to take into account the
186 exogenous factors of the slope. Following Jimenez Salas (1981), a value of $F_s \geq 1.3$ can be
187 considered stable by most standards.

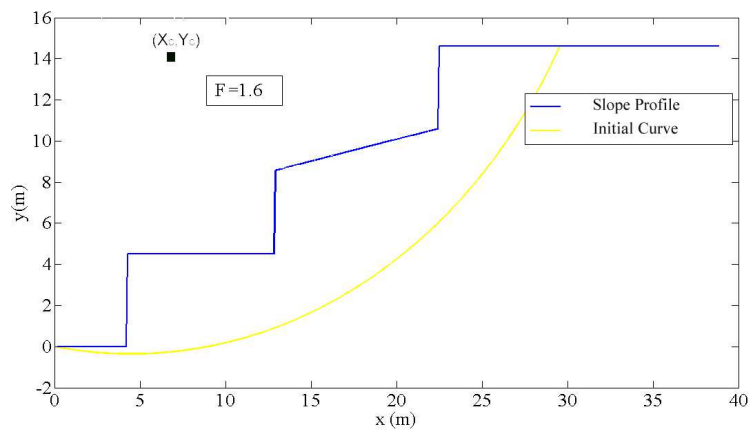
188 To analyse the slope using the Spencer's method, a set of equations must be solved to satisfy
189 the forces and momentum equilibrium and to obtain the F_s . The values of F_s and θ are the
190 unknowns that must be solved. Some authors suggest that the variation of θ can be arbitrary
191 (Morgenstern y Price, 1965), although the effect of these variations in the final value of F_s is

227 proposed by Bishop and Morgenstern (1960), the mean pore-pressure on the base of the slice
228 can be written like the equation 7.
229 This equation is used in our proposed model for calculating the safety factor (substituting the
230 expression of u in equation 5).

231 3. Terrain stability (TS) algorithm and tests

232 Figure 2 shows the results of applying the Terrain Stability model to an irregular slope,
233 including the initial and final points of the first failure circle (shown in yellow). This circle
234 corresponds with the initial value introduced by the user into the FSOLVE function. The points
235 of the slope are extracted from a DEM model in ArcGIS 10 (Glennon et al., 2008). The slope
236 height is equal to 15 m, and the soil is considered uniform with the following nominal
237 properties: $\gamma = 19500 \text{ N/m}^3$, $\phi = 22^\circ$, $c = 15000 \text{ N/m}^2$, $u = 0 \text{ N/m}^2$. For the application example
238 of our algorithm in this section, we have used Geotechnical data of a cohesive soil of the Flysch
239 type of Gibraltar, (Vallejo et al., 2002).

240 The code works as follows: the initial circular failure curve is plotted using the FPLOTT tool, as
241 shown in Figure 2 (yellow line). In this example, the center coordinates are equal to $x_c = 7 \text{ m}$;
242 $y_c = 14 \text{ m}$ and the lower cut with the slope coordinates (P1 point) equal to $x_t = 0 \text{ m}$, $y_t = 0 \text{ m}$.
243 The F_s obtained was 1.6, which is, in principle, a stable slope. It must be taken into account
244 that the mass susceptible to slipping must be divided into N pieces equal to the number of
245 slices; in this example, the mass was divided into $N = 500$ slices, the value of N is entered into
246 the user code, plus divisions of the sliding mass, more accuracy but greater need for computer
247 capacity.

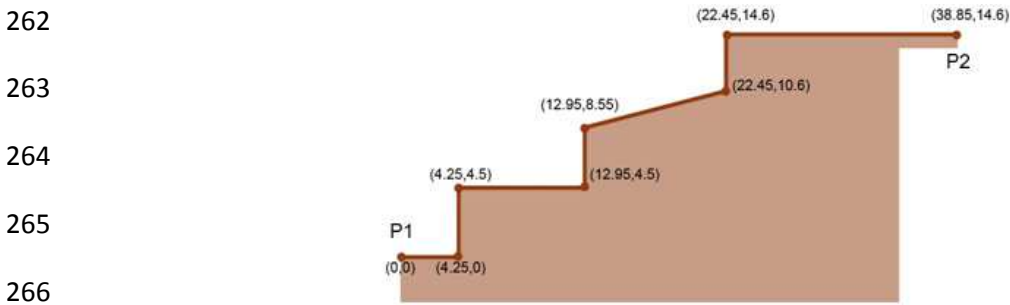


248

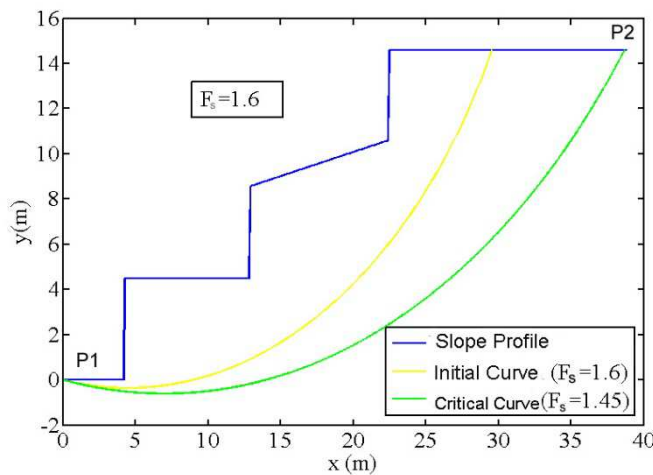
249 **Figure 2.** In this example, the center coordinates are equal to $x_c = 7 \text{ m}$; $y_c = 14 \text{ m}$, and the lower cut with
250 the slope coordinates (P1 point) equal to $x_t = 0 \text{ m}$, and $y_t = 0 \text{ m}$, data that the user introduces.

251 The next step is to apply Spencer's method to the different breakage surfaces until the curve
252 with the lowest F_s is found, and that will be the critical surface susceptible to a circular slip. To
253 determine the minimal F_s using this model, the algorithm calculates the displacement of the
254 lower cutoff point of the critical slip from the slope, as well as the position of the center of
255 rotation of the critical failure curve. In addition, the user must enter a series of possible
256 circular faults. Then, the user introduces the following constraints into the programme: the
257 initial or lower point of the failure curve (P_1) in its intersection point with the slope, which may

258 or may not match the origin of the slope analysed. Another restriction is the centre of the
 259 failure circle, (X_c, Y_c) , that should initially cut the slope, i.e. the breaking curve must be within
 260 the feasible sliding region. With this data, the programme automatically draws a first curve, in
 261 this case the yellow line in Figure 3, and calculates the safety coefficient F_s for that initial curve.



266



267

268 **Figure 3.** Results following the application of the software showing the *slope* profile and surface
 269 damage. The F_s and the clearest proof of circular failure are also provided (see the yellow line). P1
 270 coordinates are $(0, 0)$ and P2 $(38.85, 14.6)$ in metres.

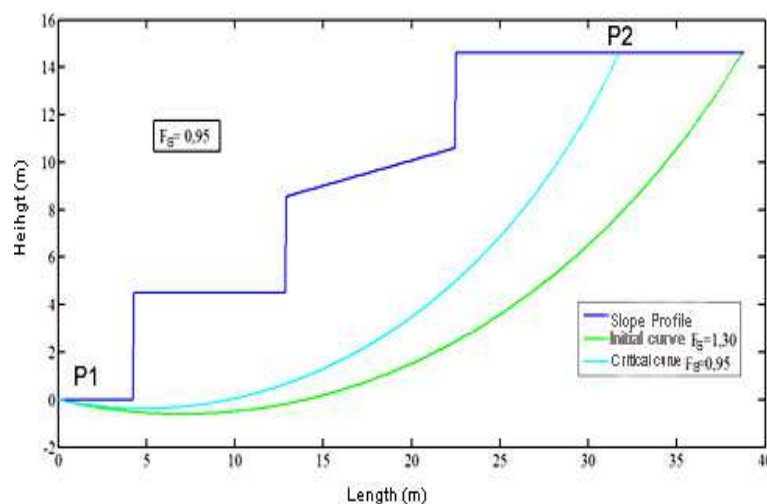
271 On the basis of this first curve (yellow line in Figure 2), the programme enforces new
 272 restrictions:

- 273 • The curve passes through the origin of slope P1 = $(0, 0)$.
- 274 • The centre of the possible circles of critical breakage is inside the rectangular box
 275 defined as: $(x_{box\ min.} < X_c < x_{box\ max.}; y_{c\ box\ min.} < y_c < y_{box\ max.})$. Note that the coordinates are
 276 entered with the 2D expression (X, Y) .

277 Both coordinates of the rotation centre position are free and can change for every circle. From
 278 the initial failure curve, characterised by the point $x = (x_c, y_c)$, the MATLAB “fmincon” function
 279 is used to obtain a new critical point (x_c^*, y_c^*) where the F_s from the breakage curve is the
 280 minimum provided by fmincon. In this example, starting from the initial curve (yellow curve)
 281 with point $x = (7, 14)$, the TS model provides a new point $x^* = (4.4910, 28.1091, 0)$ with a new
 282 F_s , $F_s = 1.45$. In this case, the new search has been carried out with the following restrictions in
 283 the rectangular box, such as $2\ m < x_c < 8\ m$ and $16\ m < y_c < 40\ m$. These restrictions are
 284 imposed in order to determine the critical circle. With all these restrictions, and because of the

285 first calculated curve (the yellow curve), the developed model calculates the critical curve
 286 among the number of curves selected by the user (500 in this case), as well as the failure circle
 287 centre, by applying the `fmincon` (MATLAB function). This defines the curve **with minimum F_s**
 288 (F_{min}) as the value of F_s (see green curve in [Figure 3](#)). When solving this problem, a critical
 289 selection is the lower cut-off point of the slope. According to different authors, such as Verruijt
 290 (2010) and Castedo et al. (2012), the selected point is the same as the P1 point.

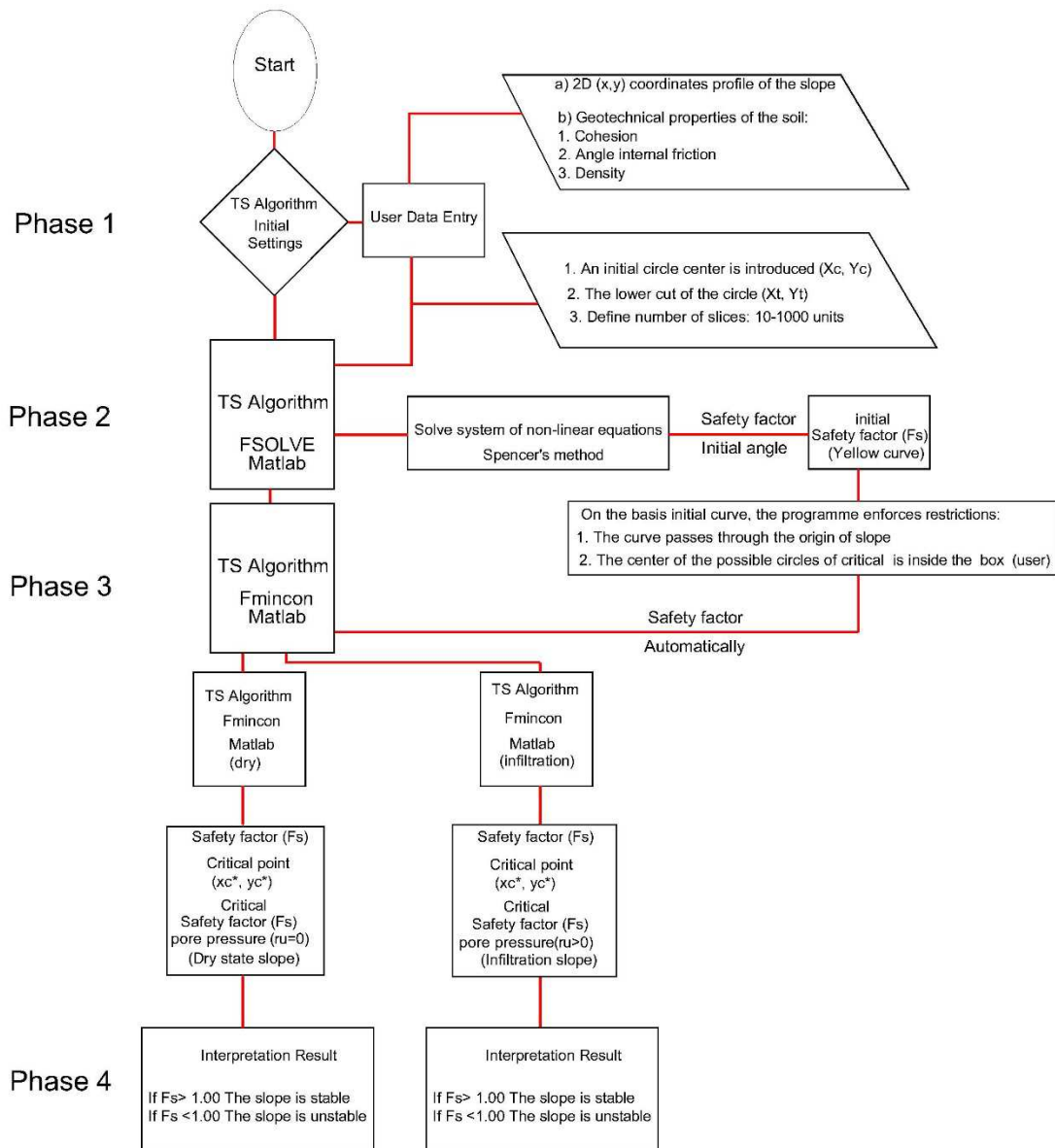
291 To complete the second phase in the TS model operation, the effect of rain infiltration must be
 292 introduced by the coefficient of the pore pressure factor r_u . In this example, the infiltration
 293 factor was introduced at the base of each slice to account for the infiltration and pore pressure
 294 at the base of the break surface of the slope. If r_u increases, the cohesion of the soil mass of
 295 the slope decreases, directly affecting the reduction of the slope's F_s . The result is that a dry
 296 slope has a $F_s = 1.45$, but if including the r_u parameter equal to 0.3, the F_s decreases to a value
 297 of $F_s = 0.95$, that means an F_s below the unity, so an unstable circular failure appears (see
 298 [Figure 4](#)). Entering the infiltration factor, r_u , in Spencer's method to introduce the infiltration
 299 effects in slopes, the geotechnical cutting elements of the analysed soil are reduced, also
 300 reducing the values of the F_s , both for the initial yellow curve and the optimum green curve
 301 ([Figure 3](#)). Note that the initial curve in the run shown in [Figure 4](#) is different from the one in
 302 [Figure 3](#), as it depends on the data introduced.



312 **Figure 4.** Outcome of the TS model after the introduction of the infiltration factor, producing an unstable
 313 circular failure ($F_s = 0.95$).

314 We can determine that if this infiltration factor value is small enough, taking into account the
 315 safety coefficients, the design may still be adequate, but critical information was missing to
 316 calculate this parameter.

317 To clarify the procedure employed in the suggested algorithm, the flowchart (block diagrams)
 318 presented in [Figure 5](#) demonstrates the calculation and iteration process as implemented in
 319 our software.



320
321
322

Figure 5. Sequential TS algorithm (block diagrams). Numbers in parentheses refer to numbers in the text.

323
324
325
326
327
328

1. Our algorithm (software) is more versatile compared to the STB 2010, the model developed here can analyze slope from right to left and vice versa, the STB 2010 only allows the analysis from right to left. Other software programmes, like the STB 2010, use a modified version of Bishop's method, a less accurate methodology than Spencer's method. A modified version of Bishop's method solves only the equilibrium in momentum while the Spencer method also considers the equilibrium in forces.

329
330
331

2. Another improvement made by the TS code, in comparison with others, is that the use of the Spencer's method allows us to analyse any type of slope and soil profile. In this procedure, we calculated the worst breaking curve by modifying the calculation points.

332 3. In the TS model, from the first slip rotational circle obtained in MATLAB, many circles
333 were then calculated using the fmincon function, with some user restrictions.
334 However, other model, like the STB 2010, require the definition of a quadrangular
335 region (to look for the centres of rotational failures) and a point (namely 5, see Figure
336 9) to define the curve as where the failure must pass. Also, the number of circles that
337 the STB 2010 model can analyse for their minimum value is limited to 100.

338 4. This model can detect relevant earth movements derived from rainfall infiltration,
339 both translational and rotational types (Stead et al., 2006), such as those that usually
340 occur in regions like India, the United States, South America and the United Kingdom,
341 among other places. The programmes that do not contemplate this option will
342 overestimate the F_s , potentially with great errors.

343 Our model programme has another advantage: it also offers the opportunity to incorporate, in
344 the same code, the stability analysis and the effect of the infiltration factor in the rainfall
345 regime. This is a step forward from open access programs, such as STB 2010, and also
346 alternative payment software, such as Slide.

347 4. Example of this application in the municipality of La Viñuela, Málaga, Spain

348 In 2010, La Viñuela, Málaga, (Spain) experienced torrential rainfall. The main consequence was
349 a devastating landslide with serious personal and material losses, as shown in Figure 6. The
350 coordinates where this event occurred were in degrees (36.88371409801, -4.204982221126).



351
352 *Figure 6. A) Spanish map with the location of La Viñuela (Google Maps). B) Real images taken by the*
353 *authors at La Viñuela in 2010.*

354 **4.1 Geological and hydrological environment**

355 The study area is located in the county of La Viñuela, specifically in the Hundidero village,
356 which is located immediately north of the [swamp of La Viñuela \(El Hundiero\)](#) and south of The
357 [Baetic System Mountain ranges \(South Iberian Peninsula\)](#).

358 According to the Cruden and Varnes' classification (1996), the slide corresponds to a rotational
359 slide-like complex movement because it was generated in two sequences at different speeds.
360 This type of mechanism is characteristic of homogeneous cohesive soils, as was the one
361 analysed here ([Cornforth, 2005](#); [Rahardjo et al., 2007](#); [Lu and Godt, 2008](#)).

362 This event caused serious damage to different buildings. Regarding the damage caused, in the
363 initial stretch of the slope (its head), a house was dragged and destroyed and another was
364 seriously damaged. On the right bank of the mentioned house, another building was affected.
365 In total, this event left a balance of two buildings destroyed and one seriously compromised.
366 Although 15 people lived in these houses, there were no fatalities. About 20 houses were to be
367 constructed at the head of the slope; fortunately, the event happened before this
368 construction. [Figure 7](#) shows an aerial picture from 2006 before the disaster as well as the
369 affected area and landslide in 2010.



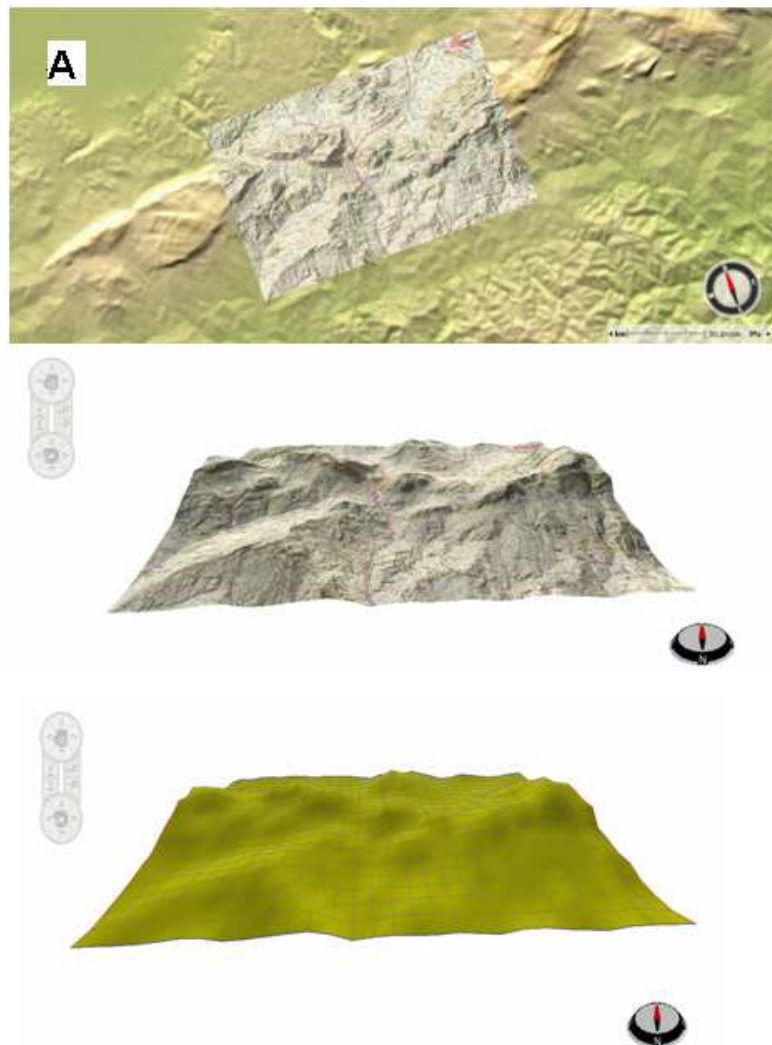
370

371 **Figure 7.** A) An aerial photograph from before the event (2006). B) An aerial photograph taken after the
372 landslide (2010).

373 **4.2 Event features and geometry**

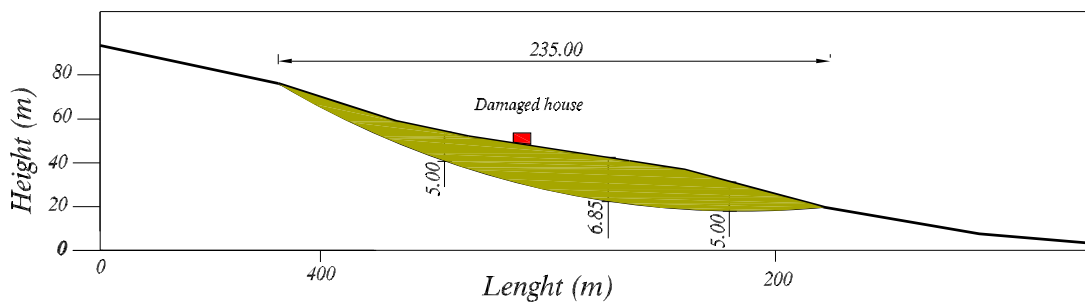
374 In this case the GIS information, we have looked for it in a map of the IGN, Spanish National
375 Geographic Institute: [websitehttp://centrodedescargas.cnig.es/CentroDescargas/index.jsp](http://centrodedescargas.cnig.es/CentroDescargas/index.jsp), in
376 this web, we have downloaded a bit map MTN25, that is a 1: 25000 topographic map in ETRS
377 89 coordinates and UTM projection. The downloaded map is generated in a file by means of a
378 geo-referenced digital rasterization (vector to raster conversion). Specifically, we downloaded
379 page number 1039, which is the one corresponding to the landslide zone of the case study.
380 The map file is generated in 'ecw' extension, file that can be opened with any GIS software, be
381 it ArcGis, Land Basic Map, among others, in figure 8 we see the topographic and raster map of
382 the case study.

383 With this map we obtain the topographic map and with this we have all the necessary profiles
384 for the study and analysis of the landslide. Moreover, as our algorithm is a 2D model, with this
385 topographic map we study the critical curve of the slip in the most unfavourable profile of the
386 landslide (Figure 8).



387
388 **Figure 8.** A) Topographic map in a GIS map; page number 1039 of the IGN (Spanish National Geographic
389 Institute).

390 It is well known that mass movements, such as landslides, are highly complex morphodynamic
 391 processes. We selected The Hundidero as our study area because it is prone to landslides. In
 392 order to analyse this case study using our model, we first calculated the initial displaced
 393 volume of the study area. According to the dimensions of the problem, the initial displaced
 394 volume was calculated, equivalent to the volume of half an ellipsoid (Varnes, 1978; Beyer,
 395 1987; Cruden and Varnes, 1996) that is $Vol = 1/6 \pi$ (width x length x depth). In our particular
 396 case, the width was equal to 70 m, the length equal to 235 m and the depth equal to 5 m,
 397 making up a total volume of 4.364 m^3 (Figure 9). Taking an average of 33% elongation, as
 398 proposed by Nicoletti and Sorriso-Valvo (1991) and Cruden and Varnes (1996), we determined
 399 that the total material displaced in this landslide had an approximate volume of 5.804 m^3 . In
 400 this mass displacement, it is also necessary to consider material added by erosion and dragged
 401 from the initial mass displaced. In Figure 7, the straight line indicates the first rotational
 402 movement, and the zigzag line shows the planar drag and glide after the first rotational
 403 movement. The green region is the total area displaced or affected by mass movement. After
 404 the first circular movement, the mass moved rapidly, associated with a continuous rise in
 405 incremental pore pressure and the rapid reduction of shear strength, without allowing
 406 pressure dissipation.



407

408 **Figure 9.** Characterisation and longitudinal section of the rotational sliding (Geolen S.A., 2010). The
 409 location of the dragged house is noted in red: Analysed by the TS model.

410

411 The initial spit of land had an approximate size of 235 m in length by 70 m in width. Due to this
 412 initial displacement, there was a drag and a huge posterior planar displacement of about
 413 550 m length, affecting a zone with several parcels of land and buildings. These sizes were
 414 confirmed using aerial photography and field data. The soil is basically composed of clays of
 415 variable thicknesses, of fine grain, with fluvial sediments and silty clay. The authors obtained
 416 this data by conducting a field survey, as well as through the laboratory tests carried out by the
 417 laboratory Geolen S.A. (Geolen, 2010). From a geological and geotechnical point of view,
 418 according to a survey of those present as the laboratory extracted the materials, different
 419 lithological levels can be distinguished, as shown in Table 1.

420

421

422

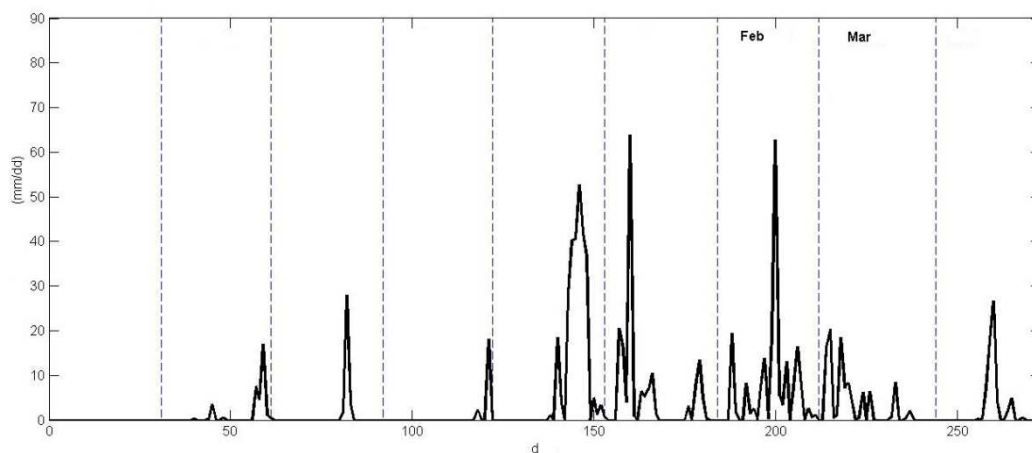
423 **Table 1.** Lithology of the area affected by the failure, according to the laboratory tests of
 424 Geolen S.A. No groundwater level was detected.

Level/layers	Lithology	Depth (m)
LEVEL 1	Silty sand with natural schistose pebbles	0.90
	Silty clay with marl intercalations	4.20
LEVEL 2	Colmenar unit, upper oligocene–lower miocene	9.00
	Sandy clay	
LEVEL 3	Colmenar unit, upper oligocene–lower miocene	(end of the probe)

425

426 The laboratory tests included a sieve analysis (following UNE 103 101) in three of the samples
 427 extracted from the field, at depths of 1.80–2.00 m, of which 70.3% was composed of clay and
 428 silt; according to this, the sample is classified as cohesive. The liquid limit and the plastic limit
 429 were determined on two of the samples (following UNE 103 103 and UNE 103 104,
 430 respectively), yielding liquid limit values of 57.5% and 64.2% and a plasticity index of 37%,
 431 respectively. According to the lab results, the material can be classified as high plasticity
 432 material with the potential of having a high water content. [The landslide analyzed began in](#)
 433 [February 2010, ending in March of that same year.](#) However, based on the field inspection and
 434 the analysis of the rainfall series in the La Viñuela region in 2010 (see [Figure 10](#)), it can be
 435 inferred that the main causes of the event were:

- 436 • The poor geomechanical parameters of the material that formed the affected hillside,
 437 and
- 438 • The hydrometeorological conditions in the days preceding and days after the event,
 439 according to the histogram.



440

441 **Figure 10.** Rainfall histogram at La Viñuela from August 2009 to April 2010. The data to make the rain
 442 histogram has been supplied by the Meteorological Agency of Spain, through the Meteorological Station
 443 of Viñuela.

444 Most of the landslides observed during these days occurred as a consequence of exceptionally
 445 intense rainfalls. The precipitation data was provided by the meteorological station of La

446 Viñuela (Figure 10). It can be observed that large amounts of precipitation fell during the
 447 months of December, January, February and March of 2010, with peaks of most 60 l/m² in a
 448 single day (January and February). In total, 890 l/m² fell in the 2009-2010 hydro cycle, which
 449 ended at the end of April 2010. This is a key point in slope stability to consider when dealing
 450 with areas capable of having high infiltration rates.

451 The rotational slide analysed had occurred between level 2 and level 3, when the water
 452 content reached that depth, as confirmed by the infiltration calculations in the terrain (see
 453 graphs in Figure 9, reaching depths of up to 5 m). Two direct shear tests (consolidated and
 454 drained) were conducted in unaltered samples extracted from the boreholes at 3.00–3.60 m
 455 and 4.00–4.60 deep. The cut-off values of the soil are specified in Table 2. Those values were
 456 used in the developed software to obtain the safety coefficient and the theoretical failure
 457 curve.

458 **Table 2.** Summary chart of the characteristics of the soil analysed at the GEOLEN S.A. laboratory: ϕ the
 459 angle of internal friction, c the cohesion, γ_{sat} the saturated specific gravity and γ_a the apparent specific
 460 gravity.

Soil parameter	Result	Units
ϕ	17	°
C	0.27	N/mm ²
γ_{sat}	2000	N/mm ³
γ_a	1650	N/mm ³

461

462 The dynamic and continuous tests were carried out by the Geolen S.A. laboratory with an
 463 automatic penetrometer ROLATEC ML-60 A type. The data obtained was transcribed by the
 464 number of strokes to advance the 20 cms tip, which is called the “penetration number” (N_{20}).

465 This test is included in the ISO 22476-2:2005 standard as a dynamic probing super heavy, and
 466 consists of penetrating the ground with a conical tip of standard dimensions. The depth of the
 467 failed mass can be estimated, as well as the theoretical failure curve for an increase in the soil
 468 consistency (see data in Table 3).

469 The change in the geomechanical response of the soil takes place at a depth of 4–5 m,
 470 according to the results of N_{20} and US (samples without changes) taken along the analysed
 471 column. In this case, the sloped ground mass showed a characteristic striking relationship of a
 472 displaced terrain (Gonzalez de Vallejo et al., 2002). This differs from the underlying or
 473 unmoved terrain, which indicated a more consistent striking relationship that was taken within
 474 the area of the landslide behind the house drawn in accordance with the analysis of the hits
 475 N_{20} from Table 3.

476

477

478

479

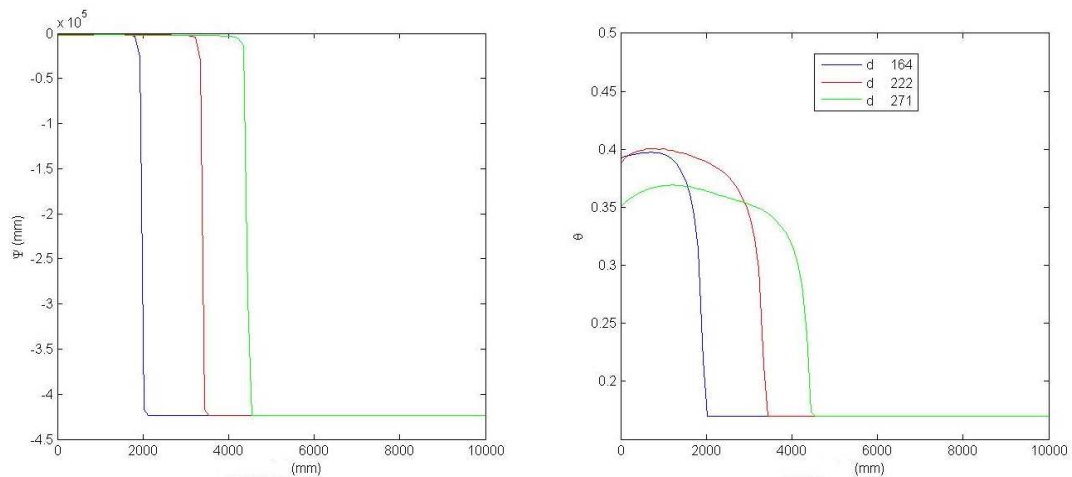
480 **Table 3.** Summary chart of the soil analysed at the GEOLEN S.A. laboratory. Bold values show, according
 481 to the data of the field penetrometers, the depth mobilized by the rotational sliding.

Depth (m)	Hits N_{20}	Consistency	Admissible stress (N/mm^2)
0.00 – 1.00	4	Soft	0.03
1.00 – 2.00	3	Soft	0.02
2.00 – 3.00	6	Slightly hard	0.04
3.00 – 4.00	7	Slightly hard	0.05
4.00 – 5.00	10	Slightly hard	0.07
5.00 – 6.00	19	Moderately hard	0.12
6.00 – 7.00	52	Hard	0.31
7.00 – 8.00	63	Hard	0.35
8.00 – 8.60	84	Hard	0.44

482

483 4.3 Input data

484 To analyse the topography of the critical section, we obtained the DEM data from ArcGIS 10
 485 software programme (Esri, 2010), with a scale of 1:1000, through Spanish National Geography
 486 Institute (IGN) raster maps, with adequate accuracy. These data were interpolated to a 2 m
 487 grid using a triangulated network interpolation methodology. Orthophotos proved very useful
 488 to locate the landslide with accuracy and to validate the field survey. The model developed
 489 here applies to failure in an initiation zone, in addition to predicting landslides, including those
 490 induced by the infiltration of critical rains.



491

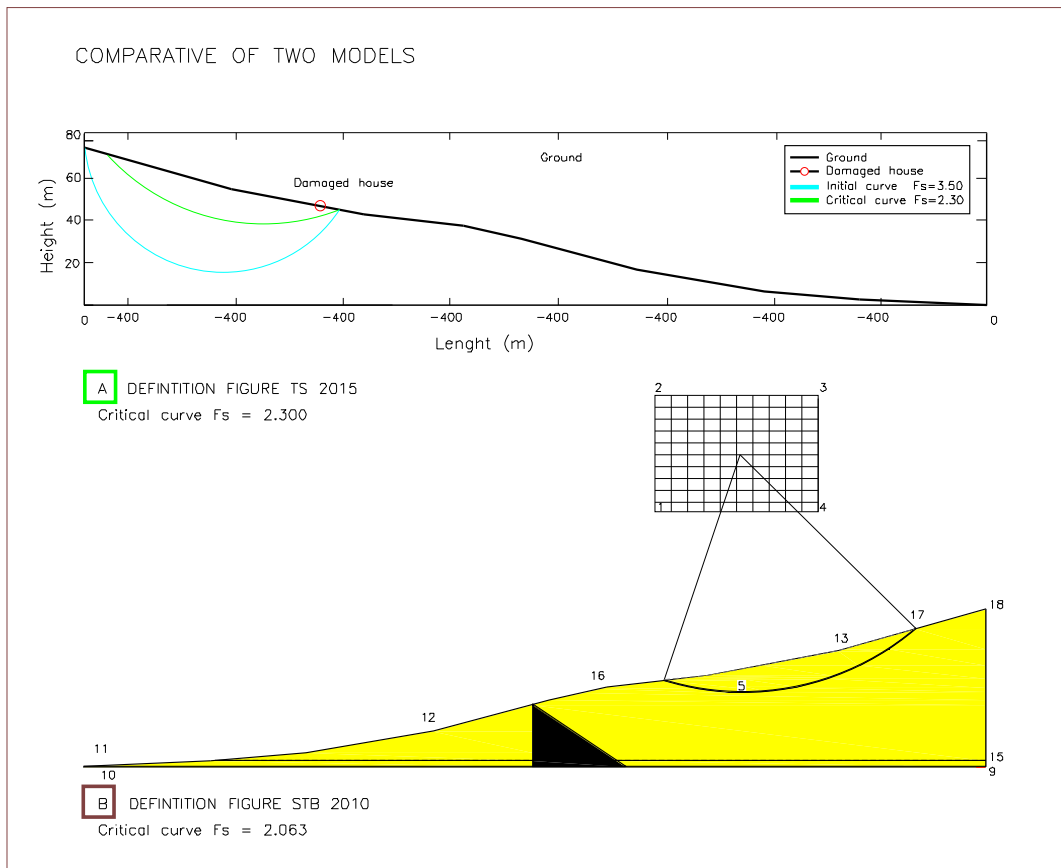
492 **Figure 11.** Left: hydraulic potential. Right: volumetric water content. Both have been plotted as a
 493 function of the depth (mm) at different times (d).

494 To complete the input data, we plotted the hydraulic potential and the volumetric water
 495 content, as a function of depth in the ground for different time steps, using a previously
 496 developed infiltration model, as shown in Figure 11 (Herrada et al., 2014). The figure shows
 497 the evolution of how the wetting front advances can be observed. These reached almost 5 m
 498 deep at the end of April 2010.

499

500 **4.2 Analytical results**

501 We applied the TS model using topographic data obtained from the ArcGIS 10 software
 502 program. We did so to obtain the degree of stability of the sliding land based on the angle of
 503 internal friction, the cohesion, the density and the angle of the slope we analyzed. Figure 9
 504 shows the analytical results from the real slope, by studying and analyzing the most
 505 unfavorable profile of the landslide studied. In addition we compared the results given by the
 506 developed TS model and the results given by STB 2010 model, using free surfaces in both
 507 cases. In our model the worst curve (shown in green) was calculated automatically from the
 508 initial curve (shown in blue), resulting in $F_s = 2.300$, in the dry state (Figure 12).

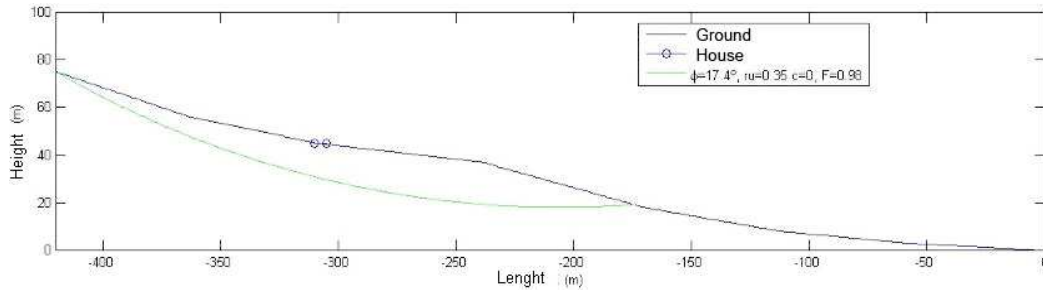


509

510 **Figure 12.** Top: TS model with a critical failure of $F_s = 2.300$. Bottom: results from the STB 2010 model
 511 with an F_s of 2.063.

512 As can be noted, the failure curves are similar, and the safety coefficients F_s only differ by
 513 0.237. In both cases, the results indicated are conservative estimates, resulting in a stable
 514 slope that was not realistic, as was the case in La Viñuela. In order to get the most
 515 unfavourable curve, which would match the analysis of the actual event, the pore coefficient
 516 must be introduced. At the first runs of the model, the r_u was equal to zero (dry soil – Figure 9),
 517 but if this value is changed to $r_u = 0.35$, the results are quite different (Figure 13). The resulting
 518 failure was near the surface and the top cut with the slope found relatively near the houses.
 519 Taking into account the infiltration of rainwater, the slope analysed in the TS model showed a
 520 value of $F_s = 0.98$, in other words, that it was unstable.

521 This calculation and the theoretical failure curve provided by our model was able to reproduce,
 522 in a realistic way, the landslide which occurred in La Viñuela. Our model found that the critical
 523 surface area that corresponded with the profile of the terrain was 12.927.45 m², which closely
 524 matches the real situation. In the STB 2010 programme, it was 7.825.35 m²; therefore, our
 525 prediction was more accurate.



526

527 **Figure 13.** A new calculation including the pore coefficient r_u showing the worst curve in green. The
 528 circles show the houses dragged by the landslide.

529 As mentioned, the STB 2010 model does not allow stability calculations to apply to rainfall
 530 infiltration on a hillside. Hence, it is not capable of predicting a hillside's instability in a critical
 531 rainfall scenario, which was critical in the slope analysed. The STB 2010 model found that the
 532 hillside studied had an F_s of $F_s = 2.063$; that means it was a very stable slope. Consequently,
 533 our original algorithm TS model appears to be more efficient and accurate.

534 If we compare the results of the penetrometric tests (Table 3) and the laboratory tests (Geolen
 535 2010) summarized in the actual critical surface in the most unfavourable profile of landslide
 536 (Figure 9), with those offered by our algorithm TS (Figure 13) to which we apply the infiltration
 537 factor $r_u=0.35$, (high interstitial pressure) we can check the similarity between the two critical
 538 surface of the landslide.

539 A value of $r_u = 0.35$ has been introduced in the calculation and the code gave us a value of the
 540 slope safety factor of $F_s = 0.95$ (unstable), when in the dry state the code calculated a safety
 541 factor of $F_s = 2.300$ (stable). The calculation of the safety factor in the STB2010 program; that
 542 lacks the analysis of infiltration in the calculation, offered a result of $F_s = 2.063$ (stable).

543 Using the STB2010 program, we would not have been able to previously detect the landslide of
 544 the case study of the paper, calculation that is not normally done in the stability calculations;
 545 with the calculation with our code we could have avoided the collapse of the building.

546 With these results, The Terrain Stability analysis performed using the developed model defines
 547 fairly well the slip-breaking curve that intuitively appears to be susceptible to failure, especially
 548 when heavy rains occur. As an example, the landslides which occurred in the La Viñuela area
 549 could only have been predicted if the infiltration had been taken into account. Even then, it
 550 could not have been done with other available software programmes, which were not able to
 551 consider it.

552 5. Conclusion

553 The terrain stability (TS) analysis defines fairly well the critical surface to landslide in 2D of
554 each profile of the analyzed slope and the safety slip factor (F_s). We developed this model due
555 to the need for a useful tool to predict landslides, especially when heavy rains occur.

556 The TS model we developed uses the Spencer's method, which is more precise than the
557 modified Bishop method, model used by other software such as the case of the STB 2010, so it
558 differs in the results it provides for the F_s . It also takes into account the factor of water
559 infiltration due to critical rains, which other software programmes do not consider. A failure
560 surface can be determined by constraints using the MATLAB function `fmincon`. The data
561 needed to run the model include soil and climate properties that may vary in space and time.
562 The exit indices of the analysis (F_s) should be interpreted in terms of relative risk. The methods
563 implemented in the TS model are based on data structures, which are based on the data entry
564 of the elevation model (DEM), [so we obtain a topographic map, a key element to obtain the
565 topographic profile to be studied with our algorithm.](#)

566 In the case study analysed, the [slope](#) was initially stable and was so determined by the analysis
567 performed with the STB 2010 model. However, the [slope](#) became unstable due to the heavy
568 rains of that hydrological period, which called for the application of the pore pressure
569 coefficient r_u . For analysing cases of heavy rain, [this model is a powerful tool](#) for determining
570 slope stability. In addition, thanks to the great versatility of this model, it is applicable to any
571 analysis in other parts of the world, based on the methods of limit equilibrium (Spencer, 1967).
572 The TS model can also be used in combination with GIS software, SINMAP, [TRIGRS model](#) and
573 aerial photographic analysis, as well as mapping techniques or even as part of other models
574 like the coastal recession models (Castedo et al., 2012).

575 6. References

576 Aenor Institut: Geotechnical investigation and testing - Field testing - Part 2: Dynamic
577 probing (ISO 22476-2:2005), Madrid, Spain, 2008.

578 [Aleotti, P.: A warning system for rainfall-induced shallow failures, Eng. Geol. 73:247–
579 265, 2004.](#)

580 [Alvioli, M., Baum, R. L.: Parallelization of the TRIGRS model for rainfall-induced
581 landslides using the message passing interface, Environmental Modelling & Software 81, 122-
582 135, <http://dx.doi.org/10.1016/j.envsoft.2016.04.002>, 2016.](#)

583
584 [Anbalagan, R.: Landslide hazard evaluation and zonation mapping in mountainous
585 terrain, Eng. Geol. 32, 269–277, 1992.](#)

586
587 [Anderson, M. G., Howes, S.: Development and application of a combined soil water-
588 slope stability model. Q. J. Eng. Geol. London, 18: 225-236, 1985.](#)

589
590 [Ayalew, L., Yamagishi, H., Ugawa, N.: Landslide susceptibility mapping using GIS-based
591 weighted linear combination, the case in Tsugawa area of Agano River, Niigata Prefecture,
592 Japan, Landslides 1, 73–81, 2004.](#)

593

594 Acharya, K. P., Bhandary, N. P., Dahal, R. K., Yatabe, R.: Seepage and slope stability
595 modelling of rainfall-induced slope failures in topographic hollows, *Geomatics, Natural Hazards*
596 *and Risk*, 7:2, 721-746, DOI:10.1080/19475705.2014.954150, 2016a.

597
598 Acharya, K. P., Yatabe, R., Bhandary, N. P., Dahal, R. K.: Deterministic slope failure
599 hazard assessment in a model catchment and its replication in neighbourhood terrain,
600 *Geomatics, Natural Hazards and Risk*, 7:1, 156-185, DOI:10.1080/19475705.2014.880856,
601 2016b.

602
603 Ayenew, T., Barbieri, G.: Inventory of landslides and susceptibility mapping in the
604 Dessie area, Northern Ethiopia, *Eng. Geol.* 77, 1–15, 2004.

605
606 Baum, R. L., Savage, W. Z., Godt, J. W.: TRIGRS-A Fortran program for transient rainfall
607 infiltration and grid-based regional slope-stability analysis, Version 2.0. US geological survey
608 open-file report 424, 38 <https://pubs.usgs.gov/of/2008/1159/>, 2008.

609
610 Bishop, A. W., Morgenstern, N. R.: Stability coefficients for earth slope, *Geotechnique*
611 10, 129-150, 1960.

612
613 Bishop, A. W.: The Use of the slip circle in the Stability Analysis of Slope, *Geotechnique*
614 5: 1:7-16, 1955.

615
616 Beyer, W. H.: *Handbook of Mathematical Sciences*. 6th ed., Boca Raton/Florida, 1987.

617
618 Bisson, M., Spinetti, C., Sulpizio, R.: Volcaniclastic flow hazard zonation in the sub-
619 apennine vesuvian area using GIS and remote sensing, *Geosphere* 10,
620 <http://dx.doi.org/10.1130/GES01041.1>, 2014.

621
622 Borselli, L.: SAPP 4.2.0.: Advanced 2D Slope stability Analysis by LEM by SSAP software,
623 SSAP code Manual, version 4.2.0, available at: <http://www.Ssap.Eu/Manualessap2010.Pdf>,
624 2012.

625
626 Burbano, G., del Cañizo, L., Gutiérrez, J. M., Fort, L., Llorens, M., Martínez, M.,
627 Paramio, J. R., Simic, D.: *Guía de cimentaciones en obras de carretera*, Ministerio Fomento,
628 Madrid, 2009.

629
630 Canili, E., Mergili, M., Thiebes, B., Glade, T.: Probabilistic landslide ensemble
631 prediction systems: lessons to be learned from hydrology, *Nat. Hazards Earth Syst. Sci.*, 18,
632 2183–2202. <https://doi.org/10.5194/nhess-18-2183-2018>, 2018.

633
634 Carrara, A., Cardinali, M., Guzzetti, F., Reichenbach, P.: GIS technology in mapping
635 landslide hazard. In: Carrara, A., Guzzetti, F. (Eds.), *Geographical Information System in*
636 *Assessing Natural Hazard*, Kluwer Academic Publisher, Netherlands, 135–175, 1995.

637
638 Casagli, N., Catani, F., Puglisi, C., Delmonaco, G., Ermini, L., Margottini, C.: An
639 inventory-based approach to landslide susceptibility assessment and its application to the
640 Virginio River Basin, Italy, *Environ. Eng. Geosci.* 3, 203–216, 2004.

641
642 Castedo, R., Murphy, W., Lawrence, J., Paredes, C.: A new process–response coastal
643 recession model of soft rock cliffs, *Geomorphology*, 177, 128-143, 2012.

641 Cheng, Y. M., Lansivaara, T., Wei, W. B.: Two-dimensional slope stability analysis
642 by limit equilibrium and strength reduction methods, *Computers and Geotechnics* 34, 3, 137-
643 150, 2007.

644 Chugh, A. K., Smart, J. D.: Suggestions for slope stability calculations. *Computers &*
645 *Structures* 14, 1-2, 43-50, 1981.

646 Collison, A., Wade, S., Griffiths, J., Dehn, M.: Modelling the impact of predicted
647 climate change on landslide frequency and magnitude in SE England. *Eng. Geol.* 55, 205-218,
648 2000.

649
650 Crosta, G. B., Frattini, P.: Distributed modelling of shallow landslides triggered by
651 intense rainfall, *Natural Hazards and Earth System Sciences* (2003) 3: 81-93, 2003.

652
653 Crozier, M. J., Glade, T.: Landslide hazard and risk: issues, concepts, and approach. In:
654 Glade, T., Anderson, M., Crozier, M. (Eds.), *Landslide Hazard and Risk*. Wiley, Chichester, 1-
655 40, 2005.

656
657 Cruden, D. M. and Varnes, D. J.: Landslides types and processes. In: *Landslides*
658 *investigation and mitigations*, Transportation Research Board Special report 24, Turner y
659 Shuster eds., 36-75, 1996.

660 CTE: Technical building Code, Basic Document Structural Safety DB-SE. Ministry of
661 Development, Spain, available at: <https://www.codigotecnico.org/>, 2007.

662 Dai, F. C., Lee, C. F.: Terrain-based mapping of landslide susceptibility using a
663 geographical information system: a case study, *Can. Geotech. J.* 38, 911-923, 2001.

664
665 Dai, F. C., Lee, C. F., Ngai, Y. Y.: Landslide risk assessment and management: an
666 overview. *Eng. Geol.* 64, 65-87, 2002.

667
668 Duncan, J. M., Wright, S. G.: *Soil Strength and Slope Stability*, John Wiley, Hoboken,
669 N. J., 2005.

670 Duncan, J. M.: *Landslide Types and Processes*. Landslides investigations and mitigation.
671 Ed. Turner A. Special Report, TRB., 1996.

672 Environmental Systems Research: Institute Geographic information system (platform
673 and resources ArcGIS), California, EEUU, available at: <http://www.esri.es/arcgis/productos/>,
674 2017.

675 Fall, M., Azzam, R., Noubactep, C.: A multi-method approach to study the stability of
676 natural slopes and landslide susceptibility mapping, *Eng. Geol.* 82, 241-263, 2006.

677
678
679 Fellenius W.: Calculation of the stability of Heat dams. Washington, D.C.: In *Proceeding*
680 *of the 2nd Internacional Congress on Large Dams*, - Vols. 4, 445. -4:445, 1936.

681 Geolen Engineering: Geotechnical study in the Viñuela. Sevilla, Spain, available at:
682 <http://www.geolen.es>, 2010.

683 Girma, F., Raghuvanshi, T. K., Ayenew, T., Hailemariam, T.: Landslide hazard zonation in
684 Ada Berga District, Central Ethiopia – a GIS based statistical approach, *J. Geomatics* 90, 25–38,
685 2015.

686 Glennon, R., Harlow, M., Minami, M., Booth, B: ArcGis 9. ArcMap Tutorial. Esri North
687 Carolina. U.S.A., 2008.

688 González de Vallejo, L., Ferrer, M., Ortuno, L., Oteo, C.: *Ingeniería Geológica*. Madrid:
689 Prentice Hall, 2002.

690 Griffiths, D. V., Marquez, R. M.: Three-dimensional slope stability analysis by elasto-
691 plastic finite elements. *Géotechnique* 57, Nº. 6, 537–546, 2007.

692 Griffiths, D. V.: Slope stability analysis by finite elements. A guide to the use of
693 Program slope 64, Geomechanics Research Center Colorado School of Mines, available at:
694 http://inside.mines.edu/~vgriffit/slope64/slope64_user_manual.pdf, 2015.

695 Guha-Sapir, D., Hargitt, D., and Hoyois, G.: Thirty years of natural Disasters 1974 –
696 2003: The Numbers, Centre for Research on the Epidemiology of Disasters, available at:
697 <http://www.unisdr.org/eng/library/Literature/8761.pdf>, 2004.

698 Gutiérrez-Martín, A.: El agua de infiltración de lluvia, agente desestabilizador de
699 taludes en la provincia de Málaga. Modelos constitutivos, Doctoral Thesis, University of
700 Granada, 2015.

701 Guzzetti, F., Carrara, A., Cardinali, M., Reichenbach, P.: Landslide hazard evaluation:
702 a review of current techniques and their application in a multi-scale study, central Italy.
703 *Geomorphology* 31 (1–4), 181–216, 1999.

704 Herrada, M. A., Gutiérrez-Martín, A., Montanero, J. M.: Modeling infiltration rates in a
705 saturated/unsaturated soil under the free draining condition. *Journal of Hydrology*, 515, 10–
706 15, 2014.

707 Hoek, E., Bray, J.W.: *Rock Slope Engineering (revised thirded.)*, Inst. of Mining and
708 Metallurgy, London, 1981.

709 Iverson, R. M.: Landslide triggering by rain infiltration. *Water Resources Research*
710 36(7): 1897-1910, 2000.

711 Janbu, N.: Stability analysis of slopes with dimensionless parameters. In: Harvard
712 University soil mechanics series, vol 46, 1954.

713 Jiménez Salas, J. A., Justo Alpañes, J.L.: *Geotecnia y Cimientos II*, Ed. Rueda, Madrid,
714 1981.

715 Jia, G. J., Tian, Y., Liu, Y., Zhang, Y.: A static and dynamic factors-coupled forecasting
716 model of regional rainfall-induced landslides: A case study of Shenzhen, Science China:
717 Technological Sciences 51. Suppl. 2, 164-175, 2008.

718 Johari, A., Mousavi, S.: An analytical probabilistic analysis of slopes based on limit
719 equilibrium methods, *Bulletin of Engineering Geology and the Environment*, 1-15, 2018.

720 Khan, M. E.: The Death Toll from Natural Disasters: The Role of Income, Geography,
721 and Institutions, *Review of Economics and Statistics* 87, 2, 271-284, 2005.

722
723 Leroi, E.: Landslide risk mapping: problems, limitation and developments. In: Cruden,
724 Fell (Ed.), *Landslide Risk Assessment*. Balkema, Rotterdam, 239–250, 1997.

725
726 Liu, S. Y., Shao, L. T., Li, H. J.: Slope stability analysis using the limit equilibrium method
727 and two finite element methods. *Computers and Geotechnics* 63, 291-298, 2015.

728 Lu, N., Godt, J.: Infinite slope stability under steady unsaturated seepage conditions.
729 *Water Resources Research*, Vol. 44, W11404, doi:10.1029/2008WR006976, 2008.

730
731 Martelloni, G, Segoni, S, Fanti, R, Catani, F.: Rainfall thresholds for the forecasting of
732 landslide occurrence at regional scale. *Landslides* DOI: 10.1007/s10346-011-0308-2, 2011.

733
734 Martelloni, G., Bagnoli, F.: Infiltration effects on a two-dimensional molecular
735 dynamics model of landslides, *Nat. Hazards*, 73(1):37–62, 2014.

736
737 Martelloni, G., Bagnoli, F., Guarino, A.: A 3D model for rain-induced landslides based
738 on molecular dynamics with fractal and fractional water diffusion, *Commun Nonlinear Sci*
739 *Numer Simulat*, 50:311–329, 2017.

740
741 Mergili, M., Marchesini, I., Rossi, M., Guzzetti, F., Fellin, W.: Spatially distributed three
742 dimensional slope stability modelling in a raster GIS, *Geomorphology* 206: 178-195.
743 <http://doi.org/10.1016/j.geomorph.2013.10.008>, 2014a.

744
745 Mergili, M., Marchesini, I., Alvioli, M., Metz, M., Schneider-Muntau, B., Rossi, M.,
746 Guzzetti, F.: A strategy for GIS-based 3-D slope stability modelling over large areas,
747 *Geoscientific Model Development* 7 (6), 2969-2982 <http://doi.org/10.5194/gmd-7-2969-2014>,
748 2014b.

749
750 Michel, G. P., Kobiyama, M., Fabris, R.: Comparative analysis of SHALSTAB and SINMAP
751 for landslide susceptibility mapping in the Cunha River basin, southern Brazil, *Journal of Soils*
752 *and Sediments* 7. 1266–1277, 2014.

753
754 Michel, G. P., Kobiyama, M., Fabris, R.: Critical rainfall to trigger landslides in Cunha
755 River basin, southern Brazil, *Natural Hazards* 75, 2369-2384, 2015.

756
757 Montgomery, D., Dietrich, W.: R-SHALSTAB: A digital terrain model for mapping
758 shallow landslide potential, to be published as a technical report by NCASI, available at:
759 <http://calm.geo.berkeley.edu/geomorph/shalstab/index.htm>,
760 [https://grass.osgeo.org/grass74/
761 manuals/addons/r.shalstab.html](https://grass.osgeo.org/grass74/manuals/addons/r.shalstab.html), 1998.

762
763 Morgenstern, N. R., Price, V. E.: The analysis of the stability of general slip surfaces,
764 *Geotechnique* 15, 79-93, 1965.

765
766 National Geographic Institute: Geological and raster maps. Madrid, Spain, available
767 at: <http://www.ign.es/web/ign/>, 2017.

764 Nicoletti, P. G., Sorriso-Valvo, M.: Geomorphic controls of the shape and mobility of
765 rock avalanches, *GSA Bulletin* 103 (10): 1365-1373, 1991.

766 Pack, R. T., Tarboton, D. G., Goodwin, C. N.: Assessing Terrain Stability in a GIS using
767 SINMAP. In: 15th annual GIS conference, GIS 2001, Vancouver, British Columbia, February 19-
768 22, 2001.

769
770 Parise, M., Jibson, R.W.: A seismic landslide susceptibility rating of geologic units
771 based on analysis of characteristics of landslides triggered by the 17 January, 1994 Northridge,
772 California earthquake, *Eng. Geol.* 58, 251–270, 2000.

773
774 Raghuvanshi, T. K., Negassa, L., Kala, P. M.: GIS based grid overlay method versus
775 modeling approach – a comparative study for Landslide Hazard Zonation (LHZ) in Meta Robi
776 District of West Showa Zone in Ethiopia, *Egypt. J. Remote Sens. Space Sci.* 18, 235–250, 2015.

777
778 Raia, S., Alvioli, M., Rossi, M., Baum, R. L., Godt, J. W., F Guzzetti, F.: Improving
779 predictive power of physically based rainfall-induced shallow landslide models: a probabilistic
780 approach, *Geosci. Model Dev.* 7 (2), 495-514, <https://doi.org/10.5194/gmd-7-495-2014>, 2014.

781
782 Ramos Vásquez, A. A.: Análisis de estabilidad de taludes en rocas, Simulación con LS-
783 DYNA y comparación con Slide, Trabajo Fin de Máster, Máster Universitario en Ingeniería
Geológica, ETSI Minas y Energía, Universidad Politécnica de Madrid, 2017.

784
785 Reid, M. E., Christian, S. B., Brien, D. L., Henderson, S. T.: Scoops-3D - Software to
786 analyze Three-Dimensional Slope Stability Throughout a Digital Landscape, Version 1.0,
787 Virginia: U.S. Geological Survey, 2015.

788
789 Rigon, R., Bertoldi, G., Over, T. M.: 2GEOtop: A distributed hydrological model with
790 coupled water and energy budgets, *Journal of Hydrometeorology* 7 (3), 371-388
791 <https://doi.org/10.1175/JHM497.1>, 2006.

792
793 Rossi, G., Catani, F., Leoni, L., Segoni, S., Tofani, V.: HIRESSS: A physically based slope
794 stability simulator for HPC applications, *Nat. Hazards Earth Syst Sci* 13(1):151–66, 2013.

795
796 Simoni, S., Zanotti, F., Bertoldi, G., Rigon, R.: Modelling the probability of occurrence of
797 shallow landslides and channelized debris flows using GEOtop-FS. *Hydrol Processes*;22(4):532-
798 545. <https://doi.org/10.1016/j.proeps.2014.06.006>, 2008.

799
800 Spencer, E.: A method of analysis of analysis of the stability of embankments assuming
801 parallel interslice forces, *Géotechnique* 17, 11-26, 1967.

802
803 Toya, H., Skidmore, M.: Economic development and the impacts of natural disasters,
804 *Economics Letters*, 94(1), 20-25. DOI: 10.1016/j.econlet.2006.06, 2007.

805
806 Tran, T. V., Alvioli, M., Lee, G., An, H. U.: Three-dimensional, time-dependent modelling
807 of rainfall-induced landslides over a digital landscape: a case study. *Landslides*, 1-14
808 <http://doi.org/10.1007/s10346-017-0931-7>, 2018.

809
810 SLIDE V5: 2D limit equilibrium slope stability for soil and rock slopes, user's guide,
811 available at: <https://www.rocscience.com/>, 2018.

809 Stead, D., Eberhardt, E., Coggan, J. S.: Developments in the characterization of complex
810 rock slope deformation and failure using numerical modelling techniques, *Eng. Geology* 83, 1-
811 3:217-235, 2006.

812 Tschuchnigg, F., Schweiger, H. F., Sloan, S. W.: Slope stability analysis by means of
813 finite element limit analysis and finite element strength reduction techniques. Part II: Back
814 analyses of a case history, *Computers and Geotechnics* 70, 178-189, 2015.

815 Van Westen, C. J., Terlien, M. J. T.: An approach towards deterministic landslide
816 hazard analysis in gis. A case study from Manizales (Colombia), *Earth Surface Processes and
817 Landforms* 21. 9:853-868, 1996.

818 Varnes, D. J.: Slope movement types and processes, In R.L. Schuster and R. J. Krizek
819 (Eds.) *Landslides: analysis and control*. Transportation Research Board. Special report 176: 11-
820 33, 1978.

821 Varnes, D. J.: *Landslide Types and Processes*. In: Turner, A.K., Schuster, R.L. (Eds.),
822 *Landslides: Investigation and Mitigation*, Transportation Research Board Special Report 247,
823 National Academy Press, National Research Council, Washington, D.C., 1996.
824

825 Verruijt, A.: STB—SLOPE: Stability Analysis Program. Delft University. Available at:
826 <http://geo.verruijt.net>, 2010.

827 Wang, X., Niu, R.: *Spatial forecast of landslides in three gorges based on spatial data
828 mining*. *Sensors* 9, 2035–2061, 2009.

829 Wilkinson, P. L., Anderson, M. G., Lloyd, D. M., Renaud, P. N.: Landslide hazard and
830 bioengineering: towards providing improved decision support through integrated numerical
831 model development, *Environment Modelling and software* 17:4, 333-344, 2002.
832

833 Wilson, R. C., Jayko, A. S.: *Preliminary maps showing rainfall thresholds for debris-flow
834 activity, San Francisco Bay Region, California*. US Geological Survey Open-File Report 97-745 F,
835 1997.

836 Wu, W., Sidle, R. C.: *A Distributed Slope Stability Model for Steep Forested Basins*.
837 *Water Resour. Res.*, 31(8), 2097–2110, doi:10.1029/95WR01136, 1995.
838

839 Yong, R. N., Alonso, E., Tabbá, M. M., Fransham, P. B.: Application of Risk Analysis to
840 the Prediction of Slope Stability. *Canadian Geotechnical Journal* 14, 540-553, 1977.

841 Zhang, S., Zhao, L., Delgado-Tellez, R., Bao, H.: A physics-based probabilistic forecasting
842 model for rainfall-induced shallow landslides at regional scale, *Nat. Hazards Earth Syst. Sci.*, 18,
843 969–982. <https://doi.org/10.5194/nhess-18-969-2018>, 2018.

844 Zhou, X. P., Cheng, H.: Analysis of stability of three-dimensional slopes using the
845 rigorous limit equilibrium method. *Eng Geol* 160:21–33, 2013.

846 Zhu, D. Y., Lee, C. F., Qian, Q. H., Chen, G. R.: A concise algorithm for computing the
847 factor of safety using the Morgenstern–Price method, *Canadian Geotechnical Journal*, Vol. 42-
848 1, 272-278, <https://doi.org/10.1139/t04-072>, 2005.